A new method to estimate the uncertainty of AEP of offshore wind power plants applied to Horns Rev 1

Murcia, Juan Pablo; Réthoré, Pierre-Elouan; Hansen, Kurt Schaldemose; Natarajan, Anand; Sørensen, John Dalsgaard

Published in:
Scientific Proceedings. EWEA Annual Conference and Exhibition 2015

Publication date:
2015

Document Version
Publisher's PDF, also known as Version of record

A new method to estimate the uncertainty of AEP of offshore wind power plants applied to Horns Rev 1

Juan P. Murcia
PhD. Student, Dept. of Wind Energy, Technical University of Denmark

Pierre E. Réthoré
Senior Researcher, Dept. of Wind Energy, Technical University of Denmark

Kurt S. Hansen
Professor, Dept. of Wind Energy, Technical University of Denmark

Anand Natarajan
Senior Scientist, Dept. of Wind Energy, Technical University of Denmark

John D. Sørensen
Professor, Department of Civil Engineering, Aalborg University

Abstract: The present article proposes a framework for validation of stationary wake models that wind developers can use to predict the energy production of a wind power plant more accurately. The application of this framework provides a new way to quantify the uncertainty of annual energy production predictions. Additionally this methodology enables the fair comparison of different wake models. Furthermore the methodology enables the estimation of how much information can be obtain from a measurement dataset to quantify model inadequacy. In the present work the proposed framework is applied to the Horns Rev 1 offshore wind power plant. The model uncertainty of a modified N. O. Jensen wake model under uncertain undisturbed flow conditions was studied. Evidence of model inadequacy is found in terms of a bias in the predicted AEP distribution. It was found that the use of the official power curve compensates the errors in the wake model, as a consequence a larger uncertainty of the overall model is predicted. Furthermore a study of wake model benchmarking based on filtered flow cases indicates that measurement uncertainty in the wind speed and wind direction is large enough to obtain any evidence of model inaccuracy even for the simplest wake models.

Keywords: Uncertainty quantification, offshore wind power plant, power predictions, wake model, SCADA data reanalysis

1. Introduction

There is a need in the wind energy industry for better predictions of wind farm power production. In particular investors and financial institutions are interested in understanding the uncertainty of production predictions in order to help them take better decisions about investing in a particular wind energy project. Previous efforts for wake model benchmarking and validation using offshore wind plant supervisory control and data acquisition (SCADA) data have been performed in the past, some examples are the work of Barthelmie et. al. [1], Hansen et. al. [5], Gaumond et. al. [4], Peña et. al. [12], Réthoré et. al. [13] and Moriarty et. al. [10] . These studies were based on the filtering of the measurements database into wind speed and wind direction bins, also called flow cases. All the publications pointed out that due to the large uncertainties in the inflow conditions it has not been possible to obtain statistical evidence about model inaccuracy. Furthermore the large number of wake models that have been evaluated produce a wide spread of power production predictions for apparently simple flow cases.

In general filtering of SCADA databases is still a common practice and uncertainties in the inflow conditions are usually disregarded. The limitations of filtering the flow cases in terms of wind direction uncertainty has been studied in Gaumond et. al. [4]. It was concluded that for large enough wind direction bins (around 30 [deg]) an accurate prediction of the mean power production can be done even with the most simple models. In contrast for narrow wind direction bins, the power production can not be accurately predicted if the wind direction uncertainty is neglected. Additionally the flow cases that have been used in the literature reduce the observed data to only the very few cases in which all the wind turbines (studied) are available and under normal operation. Réthoré et. al. [14] reported that for a wind power plant with 80 turbines only between 9 to 20% of the observations can be used. This limited number of observations has made it challenging to conclude about the uncertainty in annual energy production (AEP) predictions due to the low representation of the flow cases observed in which all turbines are under normal operation.

1.1. Objectives of the present study

The present study has the following objectives:

(1) To map the wake model prediction error for a given wind power plant energy production as a function of the uncertain undisturbed flow conditions.

(2) To estimate the wake model uncertainty to predict the mean power production of a given wind power plant when there is measurement uncertainties in each variable.

(3) To estimate the uncertainty of AEP of a given wind power plant. It is important to remark that in the present work uncertainty in AEP refers to the probability density function or distribution of possible annual energy production and not just the standard deviation around its expected value.

1.2. Model validation under uncertainty

The present work follows the framework for verification, validation and uncertainty quantification of computer codes presented by Roy and Oberkampf [15]. This framework is very relevant for wind energy since it proposed a division

between epistemic uncertainty (uncertainties that are due to lack of knowledge but that could be reduced e.g. individual measurement uncertainties, statistical uncertainty due to limited sample size and model uncertainty) from the aleatory uncertainty (uncertainties that can not be reduced e.g. real wind speed and real wind direction distribution during a time period). In this framework multiple realizations of the epistemic uncertainty of the inputs are sampled for each individual realization of the aleatory uncertainty of the inputs. By evaluating the model in each of this cases one can predict a set of distributions of the output. A similar approach is done for the possible realizations of the observed output: multiple realizations of the epistemic uncertainty are sampled for each realization of the aleatory uncertainty of the output. Roy and Oberkampf [15] and Ferson et. al. [3] have proposed the use of the area validation metric to compare the distributions of model predictions and measured outputs under measurement uncertainty. These articles argue that the area validation metric is a good estimator of the model uncertainty. In order to study the impact of measurement uncertainty and model uncertainty in the prediction of AEP it is important to be able to separate the natural (aleatory) variability of the flow resources from the measurement (epistemic) uncertainty of each individual 10-minutes measurement.

2. Methodology

2.1. Inputs/output measurements

The SCADA data was processed following the methodology for data reinforcement that has been described by Réthoré et. al. [14] in order to remove calibration shifts through time. In particular nacelle position sensors tend to have calibration shifts due to the inability to use magnetic north tracking close to large generators. Turbines are forced to perform a full 360 [deg.] turn to recalibrate the nacelle position signal. It is important to recognize that an individual turbine yaw angle signal is not an accurate estimator of the undisturbed wind direction. The settings of the yaw controllers are not known and therefore the yaw signal contains yaw errors and time dependency (filtering) due to the controller reaction time. The present work assumes that a large scale averaged undisturbed wind direction can be estimated from multiple yaw sensors, because the individual yaw errors of each turbine compensate each other.

Wind speed

The undisturbed wind speed (WS) was estimated using the average of the nacelle anemometers on the free flow operating turbines at each 10-minutes period. This average represents a spatially averaged undisturbed wind speed. Individual signals were checked for measurement quality before the averaging process was applied, which means that the number of available wind speed signals varied for each 10-minutes. The quality check consisted in comparing each individual upstream nacelle anemometer with the raw spatially averaged undisturbed wind speed. Periods that showed uncommon behavior (time increasing standard deviation) were removed.

Two additional corrections were applied to the undisturbed wind speed based on multiple nacelle anemometers. The nearby met masts hub height anemometers were used to fit a non-linear nacelle transfer function (NTF). This transfer function was used to correct the estimated wind speed for flow distortion due to the nacelle geometry and due to blade shadowing. The procedure followed is inspired in the procedure described in the IEC standard 64100-12-2 (2013) [7]. The difference with respect the standard lies in the fact that the spatial average undisturbed wind speed was used instead of a single nacelle located anemometer.

Finally an air density correction was applied following the IEC standard 64100-12-1 (2005) [6]. This correction scales the wind speed by the ratio of the current air density (10-min. mean) and the standard atmosphere air density to the one third power. This correction is recommended for normalization of power/wind speed measurements for pitch controlled wind turbines [6]. The 10-minutes mean density was estimated following the IEC standard and used the 10 min. mean barometer, air temperature, and water temperature signals.

The elicitation of the uncertainty of the undisturbed wind speed was done following the IEC standard [7]. The sources of uncertainty considered are shown in table 1. The air density correction uncertainty is the result of propagation of barometer, temperature and humidity measurement uncertainties trough the air density correction equation [7]. The large scale structures uncertainty was predicted using the trend inside the 10-minutes by computing the difference between the two consecutive undisturbed wind speeds [11]. All sources of uncertainty were assumed to be independent and normally distributed. It is important to remark that the uncertainty is estimated for each individual 10-minutes period.

Source	Type	Ref.
Calibration	B	[7]
Operation	B	[7]
Mounting	B	[7]
Data acquisition resolution	B	[7]
NTF correction	B	[7]
Air density correction	B	[7]
Large scales structures	B	[11]
Statistical	A	[7]

Table 1: Sources of uncertainty in spatially averaged undisturbed wind speed.

Note that type B uncertainties need to be normalized by applying a coverage factor of $1/\sqrt{3}$. The total uncertainty was evaluated using eq. 1 (this equation uses a general notation for any measured variable x). In this equation the left term contains the type A uncertainty estimated using N sensors and the term on the right is the combination of multiple type B uncertainties. Finally the real value of the wind speed is assumed distributed normal around the average of the multiple sensors, eq. 2 (this equation uses a general notation for any measured variable x).

$$U_x^2 = \left(\frac{std(x)}{\sqrt{N}}\right)^2 + \sum\left(\frac{U_{Bi}}{\sqrt{3}}\right)^2 \quad (1)$$

$$x_{real} \sim Normal\,(\bar{x}, U_x) \quad (2)$$

Wind direction

The undisturbed wind direction was estimated using the average of the nacelle positions signals of the free wind operating wind turbines. Individual signals were checked for calibration shifts [14] and for quality of the measurement. Each individual upstream nacelle position signal was re-calibrated based on the wind power plant layout and the power deficit of the first wake operating turbine. This procedure has been introduced by Réthoré et. al. [14].

The spatially averaged undisturbed wind direction (WD) obtained from the average of the multiple available nacelle positions showed a dependency on the wind speed. A correction based on the bias between WD and the wind vane at hub height at the nearby meteorological masts was fitted through a non-linear transfer function following the recommendations presented in the IEC standard 64100-12-2 (2013) [7]. The correction for the wind direction consisted in removing the bias as a function of wind speed.

The elicitation of the uncertainty of the undisturbed wind direction followed the IEC standard [7] and is estimated for each individual 10-minutes period. The sources of uncertainty considered are shown in table 2. The total uncertainty was calculated using eq. 1, while the real value of the wind direction is assumed normally distributed, eq. 2.

Source	Type	Ref.
In-situ re-calibration	B	[7]
Yaw signal resolution	B	[7]
Data acquisition resolution	B	[7]
Sensor alignment	B	[7]
NTF correction	B	[7]
Large scales structures	B	[11]
Statistical	A	[7]

Table 2: Sources of uncertainty in spatially averaged undisturbed wind direction.

Power

The total power production was computed by assuming that the turbines not available under normal operation produce null power. Furthermore it was assumed that a considerable reduction of the thrust coefficient occurs under down-regulation and that the wake deficits can be neglected. The power measurement uncertainty is estimated for each 10-minutes observation following the standard [6]. The sources of uncertainty considered are shown in table 3. The total uncertainty was calculated using eq. 1, while the real value of the power is assumed normally distributed, eq. 2.

Source	Type	Ref.
Calibration	B	[7]
Current transducer	B	[7]
Voltage transducer	B	[7]
Data acquisition resolution	B	[7]

Table 3: Sources of uncertainty in power measurements.

Power curve

The present study used two different power curves: the official power curve and the experimental power curve. The experimental power curve was obtained following the recommendations of the IEC standard [7]. Since SCADA databases include a large number of turbines the experimental power curved was obtained by aggregating multiple upstream wind turbines power measurements as a function of the undisturbed wind speed (for a valid wind direction sector).

Availability

The prediction of normal operation was performed individually to each turbine following the outlier detection methodology presented in [14]. This procedure used the pitch angle and normalized power curve in order to detect when a turbine is not under normal operation conditions. The obtained wind turbine availability is a combination of the actual availability, down regulation conditions and measurement sensor errors.

2.2. Modeling

Wake model

The present work could be applied to any wake model. The wake model used in the present study is a modified N. O. Jensen (NOJ) model [8]. The modified NOJ model was selected for its simplicity and because it is a model still used in the industry. The model assumes a linear wake expansion coefficient (k_j) of 0.05 for offshore conditions. In contrast to the original NOJ model, the modified model includes a near wake expansion from 1-D momentum theory occurring at the rotor disc; further more the wake deficits are scaled by the local hub height wind speed at the wake generating wind turbine instead of the undisturbed wind speed. Finally the wake deficits are aggregated with linear superposition. The model used in the present study is open source and is available at https://github.com/DTUWindEnergy/FUSED-Wake along other wake models such as the original NOJ [8] and G. C. Larsen semi-empirical wake model [9].

The model used in this study has as inputs the undisturbed wind speed, the undisturbed wind direction, the power and thrust coefficients curves, the wind power plant layout, the linear wake expansion coefficient and the availability for each turbine. As a result the model predicts the power produced by each turbine.

It is important to note that the model was executed for each of the 10-minutes inputs. The wake model was run assuming that the unavailable turbines are not running (for which the idle thrust coefficient was used) during the 10-minutes period.

Propagation of input uncertainties

A Monte Carlo simulation based on LHS sampling was used to study the effect of input uncertainty in the power distribution prediction. Each 10-minute distribution of the real wind direction and wind speed are considered independent due to their epistemic nature [15]. 100 different possible realizations of the real undisturbed flow conditions during the 3 years of analysis were calculated. This enabled to separate the aleatory component of the wind resources from the epistemic uncertainty of the measurement/estimation of undisturbed flow conditions. The present approach can be summarized as a full time series reanalysis with detailed availability and uncertainty for each 10-minutes period.

Power measurement uncertainty sampling

A Monte Carlo simulation based on a 100 LHS sample was used to study the effect of the measurement uncertainty in the observed power distribution. This approached produced 100 possible realization of the real active power through the three years of analysis.

2.3. Model validation

Area validation metric

A validation metric describes a methodology to compare an experimental distribution of a variable (with measurement uncertainty) with the result of the propagation of input measurement uncertainties through a model. In the current work the area validation metric was used to characterized the error in the prediction of the expected power of the wind power plant (U_{model}). The area validation metric quantifies the model uncertainty by comparing the median rank based cumulative density function (CDF) of the measured and predicted powers, and not only their mean values [3].

Due to the (epistemic) measurement uncertainty, the CDF of the total power measurements is defined as the region between the worst and best realization of the real power. Similarly when the uncertainty in the inputs is propagated through the model then the predicted CDF of total power becomes the region between the worst and best realizations of the model. The area validation metric is the absolute area between the two regions. If there is no are between the two regions there is no evidence of model uncertainty. This could mean that the model is very accurate or that there is too much uncertainty in the inputs. In the present work several comparisons of flow cases were done that illustrate how to use this validation metric in power production and annual energy production predictions.

The area validation metric is used to predict the confidence interval of any quantile of the output [15]. Therefore it can be used to estimate the expected model error in the prediction of the annual energy production. It is important to understand model uncertainty as an epistemic uncertainty, this means that it produces uncertainty around the predicted distribution of power. This means that it captures an additional uncertainty in the prediction of power that is independent of the input uncertainties. Figure 1 shows an example of area validation metric applied to two models that use the mean wind speed to predict the mean power. It can be observed that there is measurement uncertainty that causes the distributions to be regions. It can be seen that the model on the left gives a better estimation of the mean power (at CDF(P)$= 0.5$), but both models are equally bad at modeling the power distribution. It is expected that such models will deviate significantly from case to case depending on the actual wind resources. Therefore the model uncertainty should be similar for both models. The area validation metric in both cases is around 45 [MW]. Finally the confidence interval that includes the mean power can be estimated as the distribution obtained by the input uncertainty propagation (blue region at CDF(P)$= 0.5$) and an additional bias (uniformly distributed) given by the validation metric:

$$\mathbb{E}(P_{WF\,real}) \in \overbrace{PDF(\mathbb{E}(P_{WF\,model}))}^{\text{Input Unc.}} \pm \overbrace{U_{model}}^{\text{Model Unc.}} \quad (3)$$

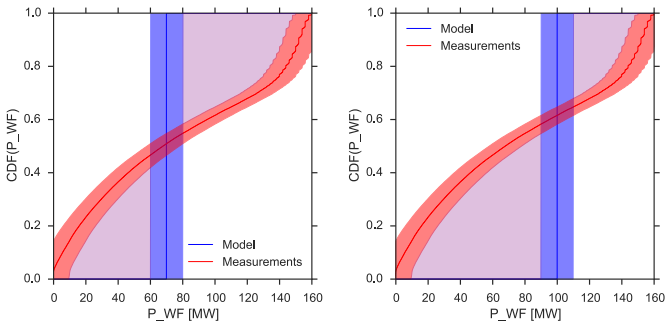

Figure 1: Example of area validation metric for CDF(P) for two models that use the mean wind speed to predict the mean power. First model prediction: $\mathbb{E}(P_{WF\,real}) \in [60, 80] \pm 45 = [15, 125]$ [MW]. Second model prediction: $\mathbb{E}(P_{WF\,real}) \in [90, 100] \pm 45 = [45, 145]$ [MW].

Boot-strapping AEP

In the present work the classical bootstrap technique [2] was used to predict the probability distribution of AEP. This technique consists in building a sample of artificial but probable years of climate, therefore it is sampling the variation (aleatory uncertainty) of the undisturbed wind. A single realization of a year was built by randomly picking a year out of the three available in the database for each of the 10-minutes periods in a given year. This was done keeping the date and time for the observation. The wind speed, wind direction, measured power, predicted power, and its respective uncertainties were chosen together. The statistical uncertainty due to a limited number of bootstrap sample was studied by following the convergence in the standard deviation of the AEP.

The bootstrapped sample is representative of the actual climate as it contains all the long term correlations such as the daily, the synoptic (high and low pressure driven patterns) and seasonal variations. The bootstrapped sample was used to evaluate the distribution of possible AEP. Finally the area validation metric based on CDF(P) was used to predict the confidence interval for the AEP. Note that this validation metric considered the area validation metric for $\mathbb{E}(P_{WF})$ (section 2.3) and the propagation of uncertainties in the undisturbed wind speed and direction through the model (section 2.2).

3. Results

3.1. Test case: Horns Rev 1

Horns Rev 1 is a Danish offshore wind power plant coowned by Vattenfall AB (60%) and DONG Energy AS (40%). It is located 14 [km] from the Danish west coast (fig. 2). The total rated power is 160 [MW]. The power plant consists of 80 Vestas V80-2.0 [MW] wind turbines, see figure 3. The power plant started operation in 2002 and is still operating in 2015.

The present work has been done using 3 years (2005-2007) of measurements from the SCADA database of the power plant. The database contains 10-minutes mean, max., min. and standard deviation for power, nacelle anemometer, nacelle position (orientation), pitch angle and rotational speed for each individual wind turbine. The present study also uses signals from the nearby meteorological mast (M2, M6, M7). Anemometers at 70 [m] height, wind vane at 68 [m]

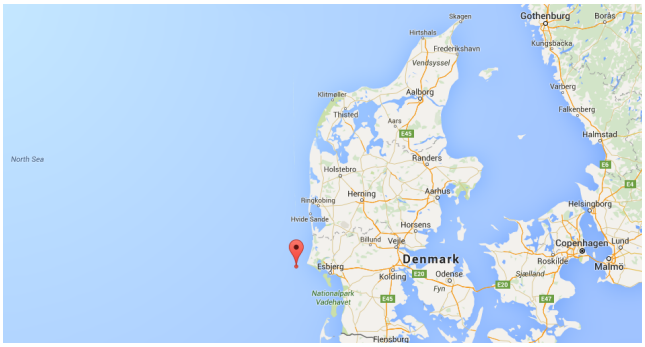

Figure 2: Location of the Horns Rev 1 offshore wind power plant. Image taken the 6th of October 2015 at http://maps.google.com.

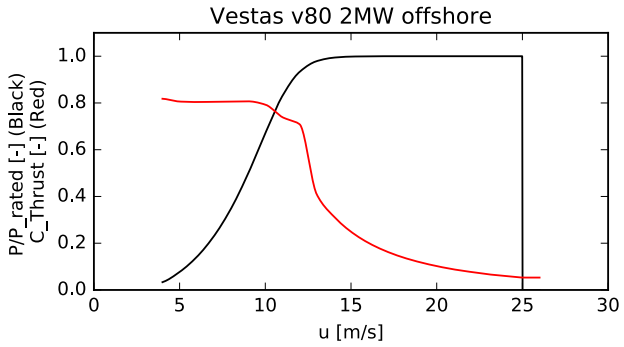

Figure 3: Vestas V80-2.0 [MW] official power curve (black line) and thrust coefficient curve (red line). April 2007 reported curves taken from the WAsP power curve database at http://wasp.dk

height, barometer sensor, air and water temperatures measurements. In the present work the available nacelle position and anemometer sensors of the free flow operating turbines were used to predict the undisturbed wind conditions. The estimation of the undisturbed wind conditions was done independently in four different undisturbed wind direction sectors, see figure 4.

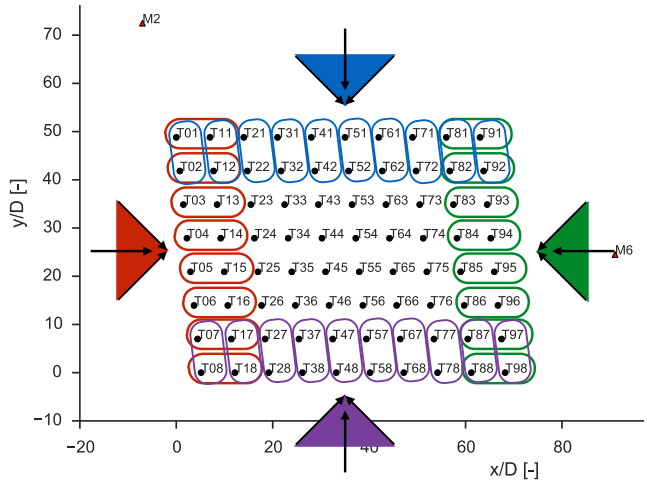

Figure 4: Selected benchmark case in Horns Rev 1. The colored area represents undisturbed wind directions. The sensors used for predicting the undisturbed flow conditions are circled and color coded.

Wind speed

Figure 5 presents an example of the transfer function correction based on the anemometer located at the top of the met mast M6 (height of 70 [m]). Note that the distance between meteorological mast and each nacelle anemometer is larger than the limit recommended in the IEC standard 64100-12-1 (2013) [7]: $4D$. Nacelle transfer functions were independently produced using M2, M6, M7 top anemometers and individual nacelle anemometers in order to asset the effect of the assumptions, similar transfer functions were obtained (not shown).

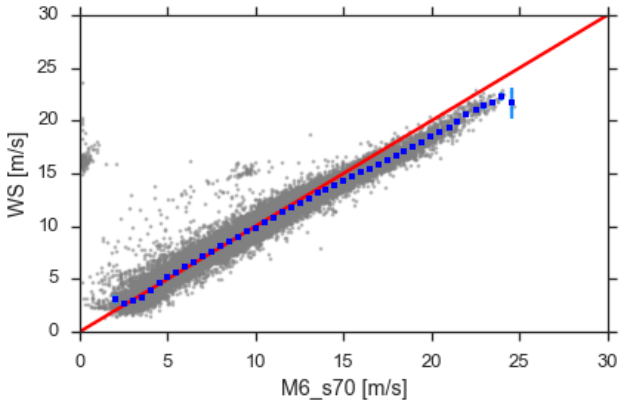

Figure 5: Nacelle transfer function between top anemometer at M6 and the large scale averaged undisturbed wind speed for the Eastern sector.

It is important to remark that the authors had not access to any information about the calibration, mounting, quality, maintenance of any of the anemometers in the wind farm. To compensate for this the uncertainty estimation is conservatively estimated. The elicitation of the uncertainty of the undisturbed wind speed is shown in table 4. This table does not present the type A uncertainty or the large scale uncertainty, since they are computed independently for each 10-min period.

Source	Type	Value
Calibration	B	0.25 [m/s]
Operation	B	class: 1.7A
Mounting	B	0.2%
Data acquisition resolution	B	0.05 [m/s]
NTF correction	B	2 %

Table 4: Estimated uncertainty in spatially averaged undisturbed wind speed.

Wind direction

An example of the nacelle position signal re-calibration based on the layout and the power deficit procedure is shown in fig. 6 for the turbines 04 and 14. In this figure the difference between the two blue lines represents the bias in the wind direction for the nacelle position senor of turbine 04.

The NTF correction for the wind direction consisted in removing the bias as a function of wind speed. Figure 7 shows the bias between the large scale averaged wind direction and the wind vane located at M6 at 68 [m] height. Similar results were obtained for M2 and M7.

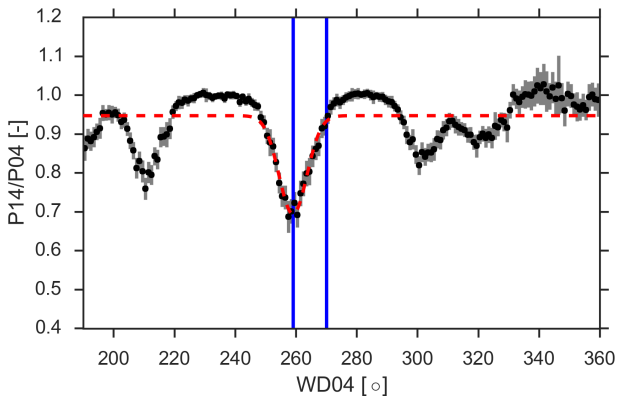

Figure 6: Nacelle position sensor for turbine 04 re-calibration based on the power ratio of turbines 14 and 04.

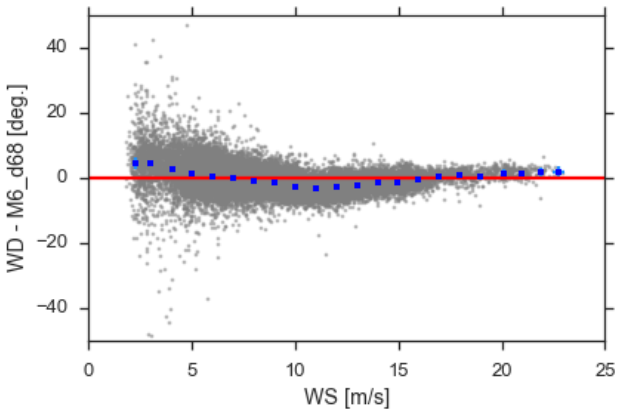

Figure 7: Undisturbed wind direction bias with respect to the wind vane at M6 at 68 [m] height as a function of the undisturbed wind speed for the Eastern sector.

A conservative elicitation of the uncertainty in the undisturbed wind direction was done following the standard for single nacelle anemometer uncertainty [7], table 5. This table does not present the type A uncertainty or the large scale uncertainty, since they are computed independently for each 10-min period.

Source	Type	Value
In-situ calibration	B	3 [deg]
Yaw signal resolution	B	2.5 [deg]
Data acquisition resolution	B	0.05 [deg]
Sensor alignment	B	1 [deg]
NTF correction	B	1 [deg]

Table 5: Estimated uncertainty in spatially averaged undisturbed wind direction.

Power

The estimated power measurement uncertainty for each 10-minutes observation is presented in table 6. Note that the power transducers have not been calibrated since installation, and it is observed that the zero power values changes between 1-2 % with reference to rated power.

Source	Type	Value
Calibration	B	2 %
Current transducer	B	2 %
Voltage transducer	B	0.9 %
Data acquisition resolution	B	2 [kW]

Table 6: Estimated uncertainty in power measurements.

Power curve

The official power curve and the multiple turbine averaged experimental power curve are presented in figure 8. Note that a simple site correction for the power curve based on the annual average turbulence intensity captures the obtained experimental power curve.

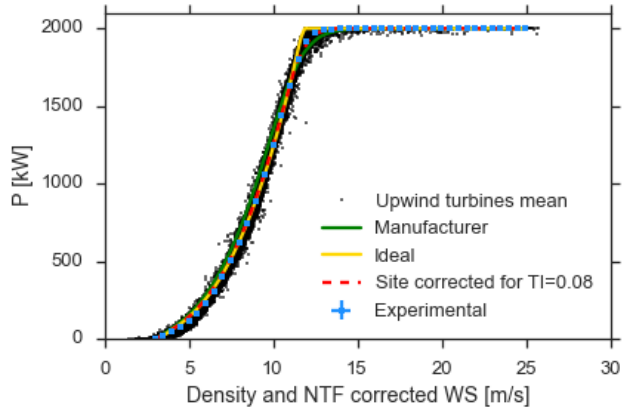

Figure 8: Official power curve and experimental power curve.

3.2. Time series of the main variables

An example of the time series of the undisturbed wind speed, wind direction, total availability, measured total power and model predicted power are presented in Figure 9. In this figure the colored areas represent the 99% confidence intervals for each of the variables. These confidence intervals include all sources of uncertainties and they should be understood as the region in which the real value lies. It is important to remark that the predicted power confidence interval is the result of the input uncertainty propagation process. This figure superficially reveals a good agreement between measurements and predictions.

Furthermore, figure 9 suggest that the confidence intervals predicted by the propagation of input uncertainty are larger than the ones caused by the measured power uncertainty. Note that the confidence intervals in the measured variables reveal that the uncertainty analysis is done for each time period. Some periods of non-available data can also be identified from this figure. Moreover the expected model prediction is build by averaging the 100 realizations of power for each 10-minutes (black line in the lower frame in figure 9).

3.3. Wind farm power rose: experimental and modeled

An example of the wind farm power rose is presented in figure 10 for a single realization of the input uncertainty during the 3 years and for a single realization of the output uncertainty during the 3 years. This figure demonstrates that

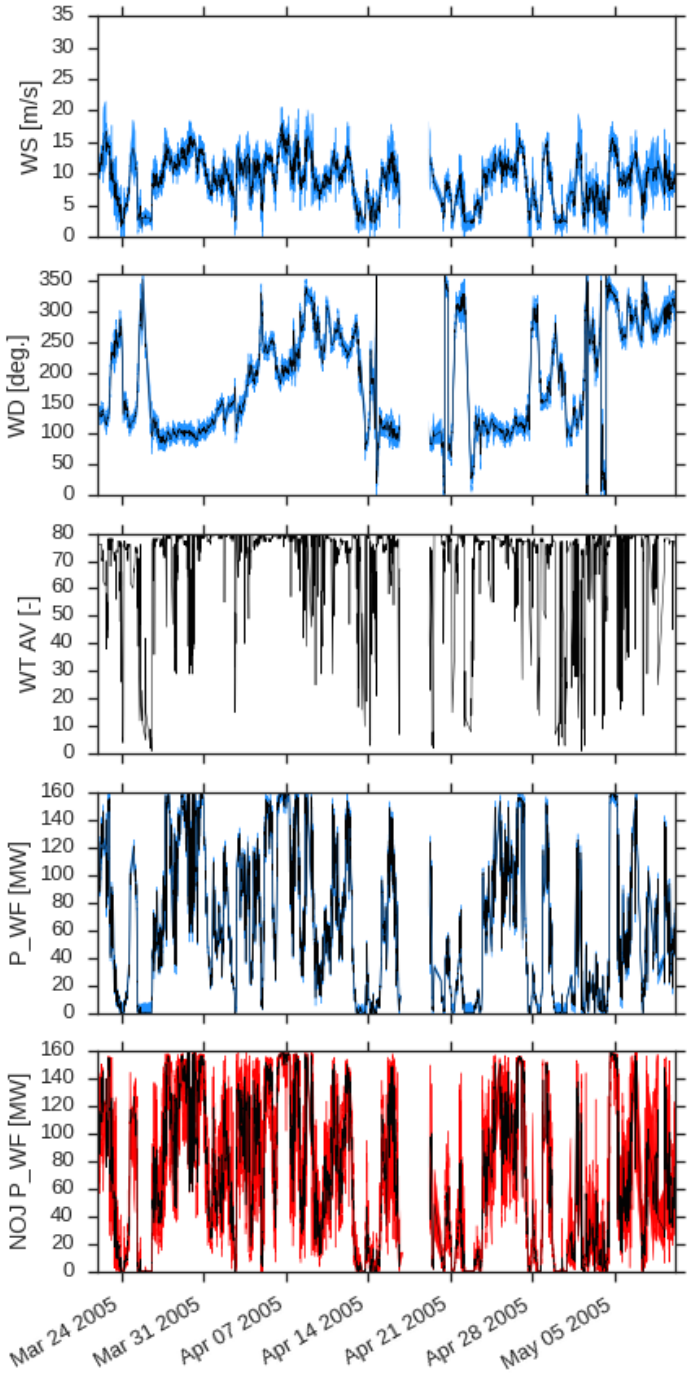

Figure 9: Example of time series of WS, WD, total availability and P_{WF} time series with 99% confidence intervals (colored areas).

the use of the actual available turbines improves the amount of data available to compare the performance of wind farm flow models.

In order to compare the level of agreement the first step is to analyze the distribution of the prediction error, see figure 11. This figure contrast the power prediction error as a function of the input variables for two cases. Using the official power curve (left frame in figure 11) produces an over-prediction of power at wind directions with less coherent wind turbine alignment; on the contrary, an under-prediction of power occurs at the wind directions of main turbine alignment. The prediction errors of the model that used the experimental power curve show a consistent under-prediction of power through the whole wind rose.

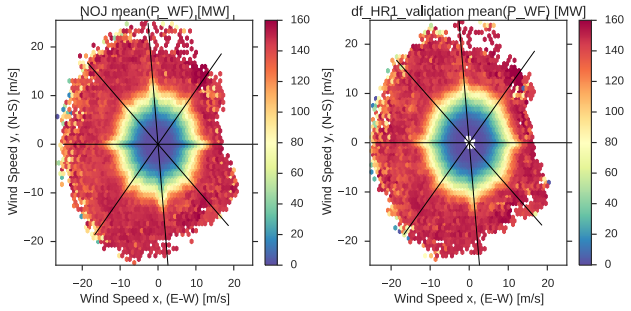

Figure 10: Wind farm power rose for (left) the model predictions based on a single realization of the inputs (right) a single realization of power measurements.

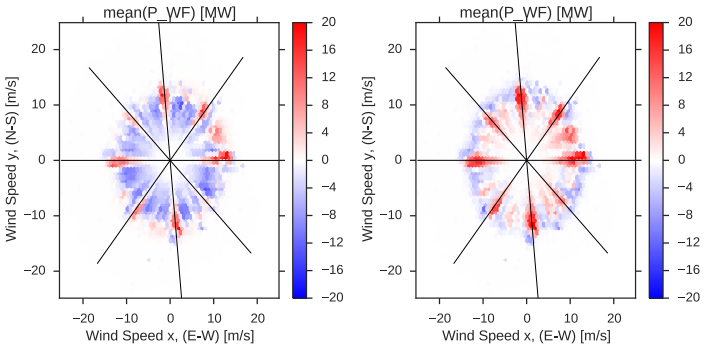

Figure 11: Power prediction error rose for a single realization of input uncertainty (left) official power curve (right) experimental power curve. Positive errors means power under-prediction (red areas) while negative errors represent power over-predictions (blue areas).

3.4. Model uncertainty for total plant expected power

The area validation metric was applied to the cumulative density function of the power, this validation metric gives an uncertainty estimation for the prediction of mean power production ($\mathbb{E}(P_{WF})$). The CDF of both measured and predicted power are shown in figure 12. Note that the CDFs presented in this figure are the areas between all the possible realization of both predicted power and measured power. It can be observed that the measurement uncertainty has negligible influence in the area validation metric. Figure 13 presents the comparison using the experimental power curve.

From figures 12 and 13, it can be observed that using the official power curve produces an over-prediction of powers below 90 [MW]. The opposite effect is observed when the experimental power curve is used: the power is under-predicted of powers below 90 [MW]. The obtained validation metrics normalized by the experimental mean power were 3% for the official power curve case, and 2% for the model that uses the experimental power curve. This suggests that the model uncertainty is lower if the experimental curve is used. The resulting model uncertainty estimations imply that using the NOJ model with the experimental power curve will

predict the actual mean power with an error of $\pm 2\%$. It is important to highlight that the area validation metric is given in absolute value, which means that it does not hold the sign of the bias. The reason for this is that due to the epistemic nature of model uncertainty, the modeler does not know before hand whether the model over-predicts the power or under-predicts it. Furthermore, the area validation metric penalizes a model that might predict the mean by compensating under-predictions with over-predictions [3].

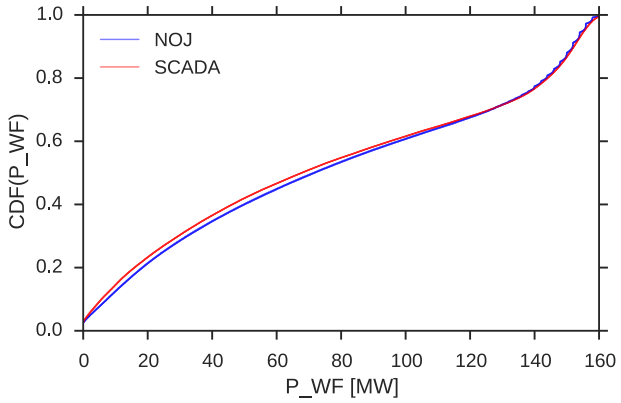

Figure 12: Area metric for CDF(P): $U_{model} = 3\% \mathbb{E}(P_{WF\,SCADA})$.

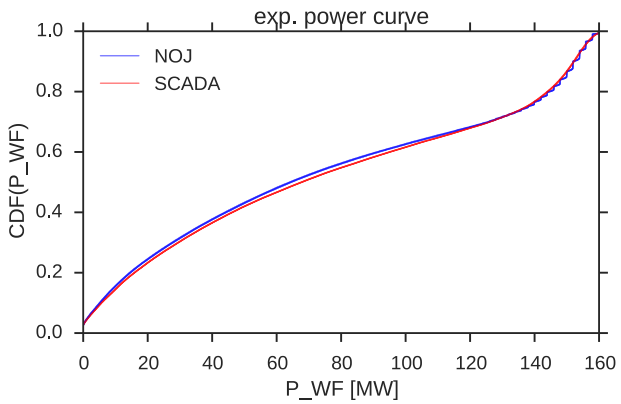

Figure 13: Area metric for CDF(P) using the experimental power curve: $U_{model} = 2\% \mathbb{E}(P_{WF\,SCADA})$

3.5. Model validation for AEP

The probability density function (PDF) of the AEP of 1000 possible years of inflow climate is presented in figure 14. This figure shows the distribution of a single realization of measurement uncertainty in the inputs (for the model), of a single realization of output uncertainty (for the SCADA database) and the aggregated distributions of AEP that include all possible realization of the measurement uncertainties. The single realization cases show peaks in the distribution which create variation in the prediction of the mean AEP (expected AEP, or P_{50}). It can also be observed that there is a bias in the model prediction of the expected AEP. This bias is due in part to the over-prediction of power caused by the official power curve. Finally it can be observed that the overall shape of the PDF of the AEP is well captured by the model. It can be concluded that the shape of the PDF of AEP only depends on the realization of the climate in the given year (bootstrapped sample).

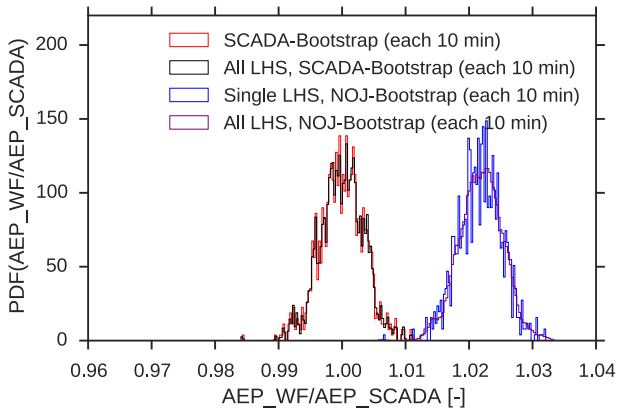

Figure 14: AEP distribution of 1000 possible years (bootstrap) with measurement uncertainties.

The final step is to combine the CDF of model AEP with the model uncertainty that was computed in section 3.4. This process is shown in figure 15. The combination of input uncertainty propagation through the model with the expected model uncertainty gives an expected range of AEP distributions. In this figure the blue are represents the range of possible CDF predicted by propagating of input uncertainties, while the green area includes the 3% model uncertainty. It can be observed that the actual distribution of AEP based on the SCADA data (red area) lies inside the predicted range (green area).

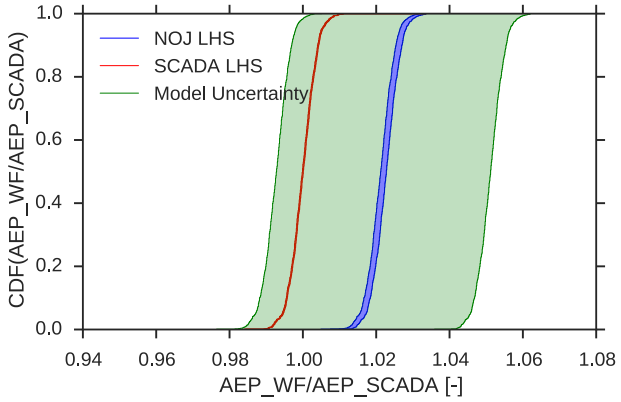

Figure 15: AEP cumulative probability distribution of 1000 possible years (bootstrap) with measurement uncertainties and wake model uncertainty.

The same procedure was repeated for the NOJ model using the experimental power curve. The probability density function of the AEP of 1000 possible years of inflow climate is presented in figure 16. This figure shows an under-prediction of the AEP. The confidence interval presented in figure 16 is a more accurate estimation of the actual bias of the NOJ model. The reason for this is the fact that the use of the experimental power curve minimizes the compensation caused by the over-prediction of the official power curve.

The combination of the CDF of model AEP with the model uncertainty is shown in figure 17 for the NOJ model with

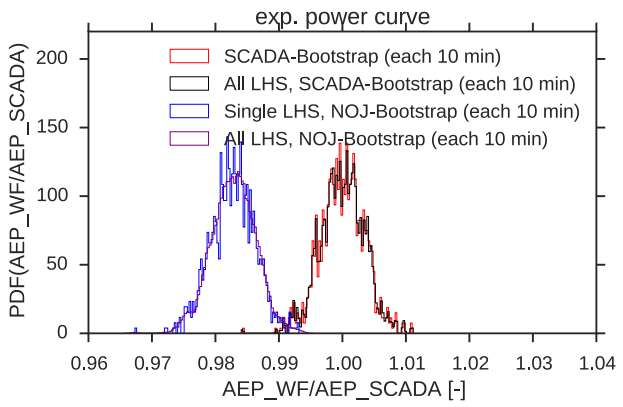

Figure 16: AEP distribution of 1000 possible years (bootstrap) with measurement uncertainties. NOJ model with experimental power curve.

the experimental power curve. The combination of input uncertainty propagation through the model with the expected model uncertainty gives an expected range of AEP distributions. It can be observed that the actual distribution of AEP based on the SCADA data lies inside the predicted region.

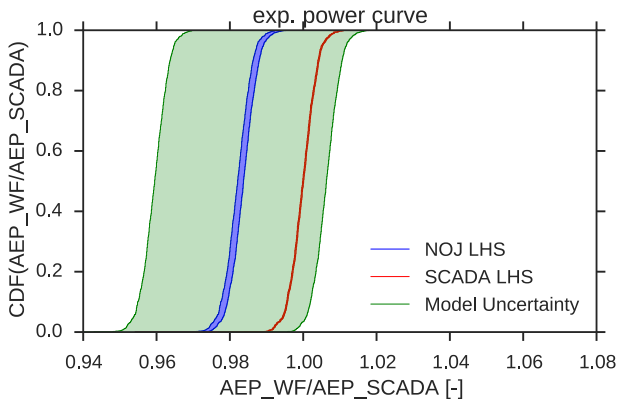

Figure 17: AEP cumulative probability distribution of 1000 possible years (bootstrap) with measurement uncertainties and wake model uncertainty. NOJ model with experimental power curve.

4. Discussion

The present framework can explain the difficulties seen in the previous wake model benchmarking campaigns. The main issue is the effect of input uncertainty in wind speed and direction in the binning process. As a consequence several of the observations obtained when filtering very narrow flow cases have actual values of wind speed and wind directions outside the bin. To show an example of the consequences of this miss-placement, the SCADA and modeled databases were filtered for an undisturbed wind direction inside [270, 272.5] [deg.] and a wind speed inside [10, 10.5] [m/s]. Figure 18 show the resulting regions of power distribution. These results reveal that due to the propagation of input uncertainty there is a null area validation metric when the model uses the official power curve. This can be interpreted as a lack of evidence of a model inadequacy in this flow case. This lack of evidence is not because of a perfect model but due to the large uncertainty in the inputs of the model.

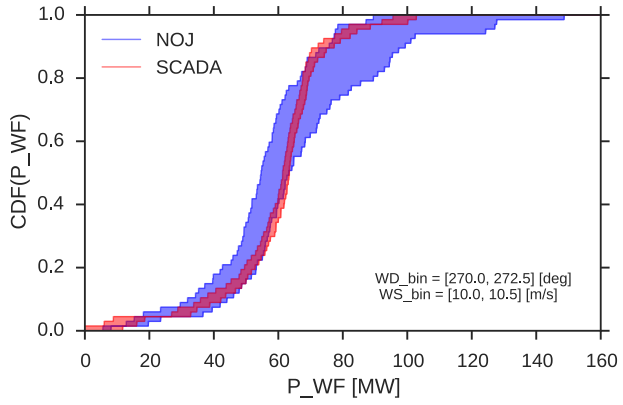

Figure 18: Area validation metric for CDF(P) for an individual flow case is null.

Figure 19 shows a similar analysis using the experimental power curve. In this case there is a relative model uncertainty of 3%. This evaluation of model inadequacy as a function of wind speed and wind direction requires to consider the measurement uncertainty in undisturbed flow conditions and in power.

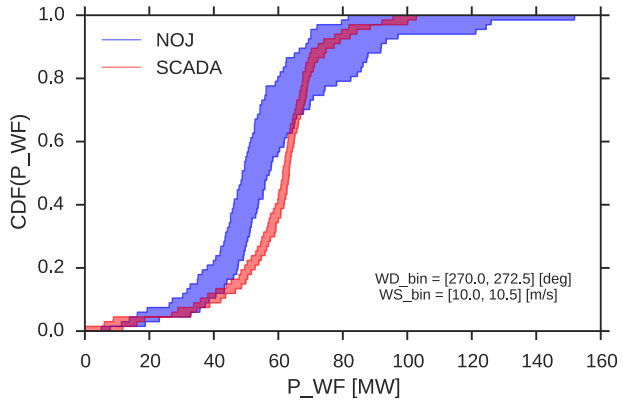

Figure 19: Area validation metric for CDF(P) for an individual flow case experimental power curve. 3%.

4.1. Further work for a full wind power plant AEP uncertainty prediction

The use of area validation metrics for power prediction distributions with uncertainty for each individual turbine inside the wind farm is planed. This study will conclude with the construction of a response surface that captures the dependency of the model uncertainty as a function of the wind speed and wind direction for each individual turbine (wake model validation region). From this results a predictive tool can be generalized such that the SCADA data from Horns Rev 1 could be use to predict the uncertainty on AEP prediction for an offshore wind power plant with an arbitrary layout. The proposed framework could be used to benchmark different wake models and to obtain individual validation regions for each model. This two aspects are the focus of the IEA-task 31.

The added uncertainty that come from modeling the power plant at full availability and by applying a percentage of operating turbines for each 10-minutes period will be studied using the area validation metric methodology. Finally the model discretization uncertainty will be quantified. This means to understand the effect of creating a wake model response database using a limited number of model evaluations.

5. Conclusions

A bias in the modified NOJ wake model prediction of annual energy production has been identified. The size and sign of this bias depends on whether the official or experimental power curve is used. The use of the official power curve makes it hard to identify the errors in the wake model, due to the errors in the turbine model. The use of the official power curve gives a larger uncertainty of the overall model based on the area validation metric of total power cumulative density function. The use of an experimental power curve or a site corrected turbulence intensity power curve indicate a lower level of superposition of turbine and wake model errors.

The standard deviation of the AEP distribution was found to be well captured by the NOJ model. It can concluded that it mainly depends on the realizations of the possible one-year wind climates and it can be more accurately predicted if the measurement uncertainty is taken into account.

Furthermore an explanation to the problem of wake model benchmarking based on filtered flow cases indicates that the measurement uncertainty in the wind speed and wind direction is large enough that there is no statistical evidence about the accuracy of the wake model if the official power curve is used. On the contrary there is statistical evidence of model inadequacy for a narrow flow case if the experimental power curve is used. Further work is planed in which the distribution of model prediction error (model uncertainty) as a function of both wind speed and wind direction for individual wind turbine power is studied.

Acknowledgments

This work was supported by the International Collaborative Energy Technology R&D Program of the Korea Institute of Energy Technology Evaluation and Planning (KETEP), granted financial resource from the Ministry of Trade, Industry & Energy, Republic of Korea. (No. 20138520021140). The authors thank DONG Energy AS and Vattenfall AB for the access to the SCADA data of Horns Rev 1.

Nomenclature

AEP	Annual energy production
CDF	Cumulative probability density function
$\mathbb{E}(x)$	Expected value of a random variable x
LHS	Latin hyper-cube sampling
PDF	Probability density function
SCADA	Supervisory control and data acquisition

References

[1] Barthelmie, R. J., Pryor, S., Frandsen, S. T., Hansen, K. S., Schepers, J., Rados, K., Schlez, W., Neubert, A., Jensen, L., and Neckelmann, S. (2010). "Quantifying the impact of wind turbine wakes on power output at offshore wind farms." *Journal of Atmospheric and Oceanic Technology*, 27(8), 1302–1317.

[2] Efron, B. (1979). "Bootstrap methods: another look at the jackknife." *The annals of Statistics*, 7(1), 1–26.

[3] Ferson, S., Oberkampf, W. L., and Ginzburg, L. (2008). "Model validation and predictive capability for the thermal challenge problem." *Computer Methods in Applied Mechanics and Engineering*, 197(29), 2408–2430.

[4] Gaumond, M., Réthoré, P.-E., Ott, S., Peña, A., Bechmann, A., and Hansen, K. S. (2014). "Evaluation of the wind direction uncertainty and its impact on wake modeling at the horns rev offshore wind farm." *Wind Energy*, 17(8), 1169–1178.

[5] Hansen, K. S., Barthelmie, R. J., Jensen, L. E., and Sommer, A. (2012). "The impact of turbulence intensity and atmospheric stability on power deficits due to wind turbine wakes at Horns Rev wind farm." *Power*, (November 2011), 183–196.

[6] IEC et al. (2005). "Iec 61400-12-1-2005 wind turbines-part 12-1: Power performance measurements of electricity producing wind turbine." *Switzerland: International Electrotechnical Commission*.

[7] IEC et al. (2013). "Iec 61400–12-2, wind turbines: part 12–2: Power performance of electricity producing wind turbines based on nacelle anemometry." *Switzerland: International Electrotechnical Commission*.

[8] Katic, I., Højstrup, J., and Jensen, N. O. (1986). "A simple model for cluster efficiency." *EWEC*, number October, 407–410.

[9] Larsen, G. C. (2009). "A simple stationary semi-analytical wake model." *Technical Report, Risø-R-1713(EN) August 2009*, Risø-DTU.

[10] Moriarty, P., Rodrigo, J. S., Gancarski, P., Chuchfield, M., Naughton, J. W., Hansen, K. S., Machefaux, E., Maguire, E., Castellani, F., Terzi, L., et al. (2014). "Iea-task 31 wakebench: Towards a protocol for wind farm flow model evaluation. part 2: Wind farm wake models." *Journal of Physics: Conference Series*, Vol. 524, IOP Publishing, 012185.

[11] Ott, S., Berg, J., and Nielsen, M. (2014). "Developments of the offshore wind turbine wake model Fuga." *Report No. DTU Wind Energy E-0046*, Risø-DTU, Roskilde, Denmark.

[12] Peña, A., Réthoré, P.-E., and Rathmann, O. (2014). "Modeling large offshore wind farms under different atmospheric stability regimes with the Park wake model." *Renewable Energy*, 70(June), 164–171.

[13] Réthoré, P.-E., Hansen, K. S., Larsen, G. C., Larsen, T. J., Ott, S., Rathmann, O., Penña, A., and Hasager, C. B. (2013). "Benchmarking of wind farm scale wake models in the eera - dtoc project." *Proceedings of the 2013 International Conference on Aerodynamics of Offshore Wind Energy Systems and Wakes (ICOWES2013)*.

[14] Réthoré, P. E., Johansen, N. A., Frandsen, S. T., Hansen, B. K. S., Jensen, L. E., and Kristoffersen, R. (2009). "Systematic wind farm measurement data reinforcement tool for wake model calibration .." *EOW Conference 2009*, 1–10.

[15] Roy, C. J. and Oberkampf, W. L. (2011). "A comprehensive framework for verification, validation, and uncertainty quantification in scientific computing." *Computer Methods in Applied Mechanics and Engineering*, 200(25-28), 2131–2144.